Energy 232 (2021) 121109

Contents lists available at ScienceDirect

Energy

journal homepage: www.elsevier.com/locate/energy

Thermodynamic performance assessment of a new solar tower-geothermal combined power plant compared to the conventional solar tower power plant

T.E. Boukelia [a, b, *], O. Arslan [c], A. Bouraoui [a]

[a] Mechanical Engineering Department, Jijel University, Jijel, Algeria
[b] Mechanical and Advanced Materials Laboratory, Polytechnic School of Constantine, Constantine, Algeria
[c] Mechanical Engineering Department, Engineering Faculty, Bilecik Seyh Edebali University, Bilecik, Turkey

ARTICLE INFO

Article history:
Received 5 December 2020
Received in revised form
14 April 2021
Accepted 29 May 2021
Available online 31 May 2021

Keywords:
Bottoming binary geothermal
Exergy
Lowtemperature
Performance
Topping solar plant

ABSTRACT

Concentrating solar power plants can be a good choice for green power generation; nevertheless, this technology has low financial profitability and energy dispatch capacities compared to those based on conventional fossil fuels. On the other side, hybridization of concentrating solar power with geothermal energy is a good option for the erection of large-scale power plants with high dispatch capacity and low investment cost, due to the large potential and geographical coincidence of geothermal resources with high solar irradiation areas. Thus, the main aim of the present paper is to investigate the hourly and annual performances of a new combined solar-geothermal power plant. This layout includes a bottoming binary geothermal power cycle that recovers the waste heat from a topping solar tower thermal power plant to generate power. In this process, both steam and organic turbines produce electrical power.

By using this new design, the dispatch capacity and annual thermodynamic performances have been raised by more than 30% compared to the conventional solar tower plant. Furthermore, the increase in geothermal production well temperature will increase the dispatch capacity of this new hybrid plant up to 152 GWh annually, for a temperature of 95 °C.

1. Introduction

There is a dramatic increase in global demand for energy due to economic trends and population growth. On the other side, the use of fossil fuel as the prime source to cater the energy needs has elevated the levels of air pollution and gas emissions. Owing to the energy demand and environmental concerns, researchers and scientists worldwide are working and exploring other alternatives and clean energy technologies for power generation. Renewable energy technologies can be a good choice in this direction; nevertheless, these technologies have often many challenges in providing a stable and reliable energy supply. These challenges are mainly driven by low financial profitability and energy dispatch capacities [1], which make them less competitive compared to those based on conventional fossil fuels.

Concentrating solar power (CSP) is one of the most promising options for large-scale power generation. This technology incorporates four different alternatives: parabolic trough thermal power plants, linear Fresnel power plants, tower power, and dish-Stirling systems. In areas suitable for the erection of CSP, sunlight usually exhibits a good match with electricity demands and its peaks. However, the available sunlight decreases to low values on cloudy or partly cloudy days, and at low sun angles in winter. Also, electricity consumption often maintains a high demand for electricity several hours after sunset. The prolongation of the capacity factor of these plants and enhancing its potential can be achieved by incorporating auxiliaries such as heat storage and/or fuel backup systems, or by developing hybrid systems by coupling CSP technology with other energy sources such as natural gas, geothermal or biomass.

Hybridization of solar technology with geothermal energy is a good option for erection of large-scale power plants with high dispatch capacity and low investment cost, due to the large potential and geographical coincidence of geothermal resources with high solar irradiation areas. For instance, available geothermal

* Corresponding author. Mechanical Engineering Department, Jijel University, Jijel, Algeria
E-mail address: taqy25000@hotmail.com (T.E. Boukelia).

https://doi.org/10.1016/j.energy.2021.121109
0360-5442/

Nomenclature

ΔA_z	Azimuth spacing between two heliostats in a row (m)
Δ_{tss}	Total number of desired storage hours (hours)
ΔR	Radial distance between two rows (m)
η_{bloc}	Optical losses in solar field due to blocking effect
η_{cos}	Optical losses in solar field due to cosine effect
η_{deb}	Losses in solar field due to overflow
η_{dis}	Losses in solar field due to dispersion
$\eta_{ene,BGPP}$	Overall energy efficiency of the bottoming BGPP
$\eta_{exe,BGPP}$	Overall exergy efficiency of the bottoming BGPP
$\eta_{ene,plant}$	Overall energy efficiency of the whole hybrid plant
$\eta_{exe,plant}$	Overall exergy efficiency of the whole hybrid plant
$\eta_{ene,STTPP}$	Overall energy efficiency of the topping STTPP
$\eta_{exe,STTPP}$	Overall exergy efficiency of the topping STTPP
$\eta_{isen,OP}$	Isentropic efficiency of the organic pump.
$\eta_{isen,OT}$	Isentropic efficiency of the organic turbine.
η_{opt}	Optical efficiency of the solar field
η_{ref}	Losses in solar field due to reflection
η_{shad}	Losses in solar field due to shading effect
θ_t	Angle between the vertical and the vector from the heliostat to the tower (°)
A_{helio}	Area of a single heliostat (m^2)
C_{HTF}	Heat capacity of the working fluid (kJ/kg.K)
CF	Capacity factor (%)
$D_{i,tube}$	Inner diameter of the tube (m)
$D_{o,tube}$	Outer diameter of the tube (m)
$\dot{E}x_{abs}$	Exergy absorbed by the solar receiver (kW)
$\dot{E}x_{geo}$	Exergy received by the geothermal plant (kW)
$\dot{E}x_{inc}$	Exergy received by the heliostat field (kW)
$\dot{E}x_u$	Useful exergy delivered by the solar receiver (kW)
f	Dilution factor ($1.3*10^{-5}$)
f_{backup}	Fossil fill fraction ($0 < f_{backup} < 1$)
h	Enthalpy at each point of the ORBPB (kJ/kg)
H_{helio}	Height of the heliostat mirror (m)
$h_{in\ turbine}$	Enthalpy at the inlet of the steam turbine (kJ/kg)
h_{SFi}	Enthalpy at the inlet of the SF (kJ/kg)
h_{SFo}	Enthalpy at the outlet solar field (kJ/kg)
I_{BN}	Hourly direct normal irradiance (kW/m^2)
k_{tube}	Thermal conductivity of the receiver tube (W/m.K)
$\dot{m}_{cw}$	Mass flow rate of the cooling water (kg/s)
$\dot{m}_{geo}$	Mass flow rate of the geothermal water (kg/s)
$\dot{m}_{of}$	Mass flow rate of the organic fluid (kg/s)
$\dot{m}_{HTF}$	Mass flow rate of the HTF (kg/s)
N_{helio}	Total number of heliostats in the field
N_{tube}	Number of the receiver tubes
ND	Number of the days in a year
$PG_{geo,net}$	Net power generation by the bottoming BGPP (kW)
$PG_{plant,net}$	Net power generation by the whole hybrid plant (kW)
$PG_{solar,net}$	Net power generation by the topping solar power plant (kW)
$\dot{Q}_{abs}$	Energy reaches the receiver surface (kW)
$\dot{q}_{conv}$	Energy loss by convection heat transfer from the receiver (kW)
$\dot{Q}_{evap}$	Energy transferred through the evaporator (kW)
$\dot{Q}_{FBS}$	Thermal energy must be supplied by the FBS (kW)
$\dot{Q}_{gain}$	Total energy gained by the bottoming BGPP (kW)
$\dot{Q}_{geo}$	Energy flow from the geothermal source (kW)
$\dot{q}_{HTF}$	Energy absorbed by molten salt heat transfer fluid (kW)
$\dot{Q}_{inc}$	Total energy incident on the heliostat field (kW)
$\dot{q}_{rad}$	Energy loss by radiation from the receiver (kW)
$\dot{q}_{ref}$	Energy loss by reflection from the surface of the receiver (kW)
$\dot{Q}_{rej,STTPP}$	The total energy rejected by the topping STTPP (kW)
R_{cond}	Heat transfer resistance by conduction through the tube wall (K/m)
R_{conv}	Heat transfer resistance by convection from the inner tube wall to HTF (K/m)
s_{SFi}	Entropy at the inlet of the SF (kJ/kg.K)
s_{SF0}	Entropy at the outlet of the SF (kJ/kg.K)
T_{amb}	Ambient temperature (K)
$T_{HTF,ave,x}$	Average temperature of the working fluid at x position (K)
$T_{HTF,\ x_0}$	Inlet temperature of the working fluid at x position (K)
$T_{HTF,\ x_0+\Delta x}$	Outlet temperature of the molten salt at x + dx position (K)
$T_{s,x}$	Receiver surface temperature at the x position (K)
T_{sun}	Temperature of the sun (K)
W_{helio}	Width of the heliostat (m)
$\dot{W}_{OP}$	Power consumed by the organic pump (kW)
$\dot{W}_{OT}$	Power produced by the organic turbine (kW)

Abbreviation

BGPP	Binary geothermal power plant
CON	Condenser
CP	Condenser pump
CSP	Concentrating solar power
DEA	Deaerator
DNI	Direct normal irradiance
DP	Deaerator pump
EVAP	Evaporator
FBS	Fuel backup system
FWH	Closed feed water heaters
GEN	Generator
HF	Heliostat field
HPT	High-pressure turbine
HTF	Heat transfer fluid
LPT	Low-pressure turbine
NREL	National Renewable Energy Laboratory
OP	Organic pump
ORBPB	Organic Rankine bottoming power block
ORC	Organic Rankine cycle
OT	Organic turbine
PB	Power block
PH	Preheater
RH	Reheater
RTPB	Rankine topping power block
SAM	System Advisor Model
SF	Solar field
SG	Steam generator
SP	Superheater
SR	Solar receiver
STTPP	Solar tower thermal power plant
T	Tower
TSS	Thermal storage system

resources are located at the boundaries of Pacific Ocean, South Europe, in addition to Africa [2]. Considering this critical motivation, hybrid solar-geothermal technologies for power generation have been investigated by researchers, and many published papers have been published in the literature. Starting by Li et al. [3], they reviewed the progress in research and development of solar and geothermal power plants, as well as the possibility of hybridization of these systems with each other. Finally, they made an assessment and classification of these systems according to their efficiencies. While Astolfi et al. [2] evaluated the techno-economic performances of a new combined CSP with a geothermal binary plant. The organic Rankine cycle (ORC) working under the supercritical phase has been designed to convert the intermediate enthalpy geothermal source to electricity, and the parabolic trough solar field is incorporated in the system, to supply more heat to enhance the dispatch capacity of the whole plant. Furthermore, off-design analysis has been considered to evaluate the yearly production of the system, and the economic dimension is also considered to determine the costs. In the same way, Zhou with his team [4] evaluated the performances of a hybrid solar-geothermal plant in terms of generated power and levelized cost of electricity and compared these performances to those of stand-alone solar and geothermal systems. Besides, the influence of different parameters such as ambient temperature, solar resource, geothermal reservoir quality on the performance of the plant was also studied. In the last section of their paper, they considered the dynamic behavior of this plant under the climatic conditions of three locations in Australia. In another study [5], the corresponding author performed another study, where the supercritical ORC has been considered to generate power from a hybrid solar-geothermal energy system. Moreover, the performances of this configuration were compared to those of stand-alone solar and geothermal plants, as well as a subcritical hybrid plant using the two technologies. The study assessed both technical and economical indicators. While Ghasemi et al. [6] developed a numerical model based on an operating low-temperature geothermal power plant working with ORC. Then, they retrofitted this plant with another low-temperature parabolic trough solar field. The developed model presented a new strategy to achieve a significant dispatch capacity compared to the classic operating geothermal binary plant. Another numerical model of a hybrid solar-geothermal power plant is performed by Ayub et al. [7]. The power plant is based on the same configuration presented by Ref. [6], and the numerical model considers both thermodynamic and economic criteria to maximize the generated power, and evaluate the performances for selected days. On the same wave, Cardemil et al. [8] presented a mathematical model to evaluate the performances of a hybrid single and double flash geothermal-solar system for large-scale power generation. The parabolic trough technology is chosen for the solar field, while four different geothermal reservoir conditions were considered for the geothermal side. The study took the 2nd law efficiency and geothermal resource consumption as objective parameters for the optimization. Motivated by the coincidence of high ambient temperatures with high levels of solar radiation, Heberle et al. [9] analyzed a solar thermal retrofit based on the superheating of organic fluid of a geothermal binary plant. The solar field is based on parabolic trough technology and working with thermic oil, while the geothermal side is based on a binary air-cooled cycle. Both technical and economical dimensions have been taken into account, and Turkish climatic conditions were chosen for the simulation. A thermodynamic analysis based on both energy and exergy models of a hybrid solar-geothermal system has been presented by Acar and Arslan [10]. For this purpose, R-600a has been chosen as working fluid in the ORC cycle, while Therminol VP-1 and molten salt have been selected as circulating fluids in the solar field and thermal storage respectively. In the same direction, more works have been published on the simulation of hybrid solar-geothermal power plants for power generation [11–19].

However, to sum up, it can be concluded that most of the previous studies are concentrated on using one of the two sources (either solar or geothermal) as a backup system to enhance the generated power and techno-economic performances of the other system. On the other hand, since there is huge waste heat from the solar thermal power plant, and the possibility of using this energy for low power generation, this study presents the design of a new combined solar-geothermal power plant. This configuration includes a bottoming binary geothermal power cycle that will recover the wasted heat from an existing solar thermal power plant to generate power. In this process, both steam and ORC turbines produce electrical power. By integrating this new solution, the use of solar and geothermal energy sources can be optimized by reducing the energy losses compared to stand-alone plants, and the technical performances will be greatly improved.

2. Data and methodology

2.1. Adopted methodology

In the present study, combining a binary geothermal power plant (BGPP) with a solar tower thermal power plant (STTPP) will be studied. Considering such a hybrid configuration will allow the geothermal source to gain wasted heat from the solar topping cycle, to boost the generated power by the bottoming organic Rankine cycle (ORC). The solar side is based on a solar tower technology working with molten salt, and incorporated with two auxiliaries; thermal storage system (TSS) and fuel backup system (FBS), which is similar to Gemasolar plant [20]. While for the bottoming geothermal side, it is based on an existing geothermal AFJET ORC power plant [21]. The main target of this study is to explore hourly and annual performances of using this configuration for large-scale power generation, in terms of design and thermodynamic yield (energetic and exergetic). Furthermore, the design of the BGPP will be optimized to match the levels of wasted heat from the topping STTPP. In this regard, the main methodology adopted in this paper includes the following main points:

- Generating meteorological data, and gathering technical data necessary to simulate the new hybrid plant.
- Present the mathematical modeling of the studied hybrid CSP-geothermal configuration. It includes the design of the main systems of this configuration, including the solar field, the two incorporated auxiliaries (TSS and FBS), and the Rankine power cycle, as well as the bottoming BGPP.
- Evaluate the performances of the new combined power plant in comparison to the stand-alone solar power plant. This evaluation will include the energy and exergy efficiencies, and considering both the hourly and annual basis.
- Optimize the mass flow rate of the bottoming ORC cycle to meet the energy flows of the topping STTPP based on yearly round simulations.

2.2. Site of the simulations

The selected site should be characterized by high solar resources and has geothermal sources of low enthalpy range. Thus, El Oued has been chosen to perform the simulations. It is located in the South-East of Algeria as presented in Fig. 1, and it is characterized by its relatively high solar resource (about a mean DNI of 5.4 kWh/m^2/day), which is an acceptable condition for the installation of

Fig. 1. Location where the simulations have been performed [22].

concentrating solar systems.

Furthermore, the chosen site contains a low-temperature geothermal source of 65 °C [23], which makes it a good match for the erection of the presented plant. The technical characteristics of the geothermal source are given in Table 1.

2.3. Studied configuration

As previously mentioned, a hybrid CSP-geothermal plant will be investigated. This configuration, including its main components, is schematized in Fig. 2. In this layout, the combined cycle technology will be considered, where the topping STTPP uses a large field of many sun-tracking mirrors called heliostat field (HF), to focus sunlight on a solar receiver (SR) located at the top of a tower (T). Thus, a reference STTPP working with molten salt, and integrated with TSS and FBS has been chosen as the topping cycle. This plant is similar to Gemasolar plant (South of Spain) with a gross capacity of 19.9 MW, which is the first commercial-scale power plant of its type. The molten salt heated in the receiver is used to generate superheated steam, which, in turn, is used in a conventional Rankine power block (PB) to produce electricity. A thermal storage system (TSS) and a fuel backup system (FBS) have been connected to the plant to provide heat whenever the thermodynamical state required at the steam turbine inlet is not accomplished, thus, raise the dispatchability of the plant. In the Rankine topping power block (RTPB), the molten salt passes through three doubled heat exchangers including superheater (SP), steam generator (SG), and preheater (PH) sections to generate high-temperature steam. To enhance the thermal efficiency of the plant, using a reheater section (RH) between high-pressure (HPT) and low-pressure (LPT) turbine sections is highly recommended. Moreover, five closed feedwater heaters (FWH) and a deaerator (DEA) have been integrated. On the other side, to circulate the liquid water coming from the condenser (CON) and the deaerator, condenser and deaerator pumps (CP, DP) have been used. On the other side, a binary geothermal power plant working with similar conditions as those of the existing AFJET geothermal power plant [21], is used as a bottoming cycle. In this plant, the hot geothermal water from the production well is pumped through the condenser (CON1) of the topping Rankine cycle to gain more thermal energy from the wasted heat of this cycle, then, to the evaporator (EVAP) to transfer heat to another fluid (organic fluid). The cooled water is returned to the re-injection well. The organic fluid (which is R134a in this study) is pumped at high pressure through the EVAP, where it is vaporized, then, expanded in the organic turbine (OT) to generate power. The vapor leaving the turbine is then condensed and cycled back.

The technical data of this plant were summarized in Tables 2 and 3 for topping STTPP with TSS and FBS, and bottoming BGPP, respectively.

Table 1
Properties of the geothermal source [23].

Property	Value
Temperature at production well [°C]	65
Temperature at re-injection well [°C]	35
Mass flow rate of the geothermal fluid (kg/s)	195
Pressure of the geothermal source [kPa]	220

2.4. Mathematical modeling

2.4.1. Topping STTPP

✓ Solar Field (SF)

As raised before, the same design of Gemasolar power plant is employed in the topping solar tower thermal power plant (STTPP). This plant is working with molten nitrate salt (60% $NaNO_3$+ 40% KNO_3) as the primary heat transfer fluid (HTF) both in the SF and TSS. The temperature-dependent correlations for different thermophysical properties such as density, viscosity, conductivity, and specific heat capacity, in addition to specific enthalpy and entropy were taken from Ref. [33] for molten salt, and [34] for water/steam (which is the working fluid in the power block). Furthermore, the heliostat field with a surrounding layout is selected, and the optimal values of the azimuth spacing (ΔA_z) and the radial distance (ΔR) have been generated using two empirical equations [35]:

$$\Delta R = (1.1442 \times \cot\theta_L - 1.0935 + 3.0684 \times \theta_L) H_{helio} \quad (1)$$

$$\Delta A_Z = (1.791 + 0.6396 \times \theta_L) \times W_{helio} + \frac{0.02873}{\theta_L - 0.04902} \quad (2)$$

where, θ_L is defined by:

$$\theta_L = \frac{\pi}{2} - \theta_t \quad (3)$$

θ_t is defined as the angle between the vertical and the vector from the heliostat to the tower, and H_{helio}, W_{helio} are denoted for the height and width of every single heliostat.

Optical efficiency η_{opt} which represents the ratio of the power that successfully reaches the receiver surface Q_{abs} to the total solar radiation incident on the heliostat field is given mathematically by Ref. [35]:

$$\eta_{opt} = \frac{\dot{Q}_{abs}}{\dot{Q}_{inc}} = \frac{\dot{Q}_{abs}}{I_{BN} \times A_{helio} \times N_{helio}} \quad (4)$$

where: N_{helio}, A_{helio}: are the total number of heliostats in the HF and the area of every single heliostat, respectively.

Moreover, several losses can adversely affect the optical

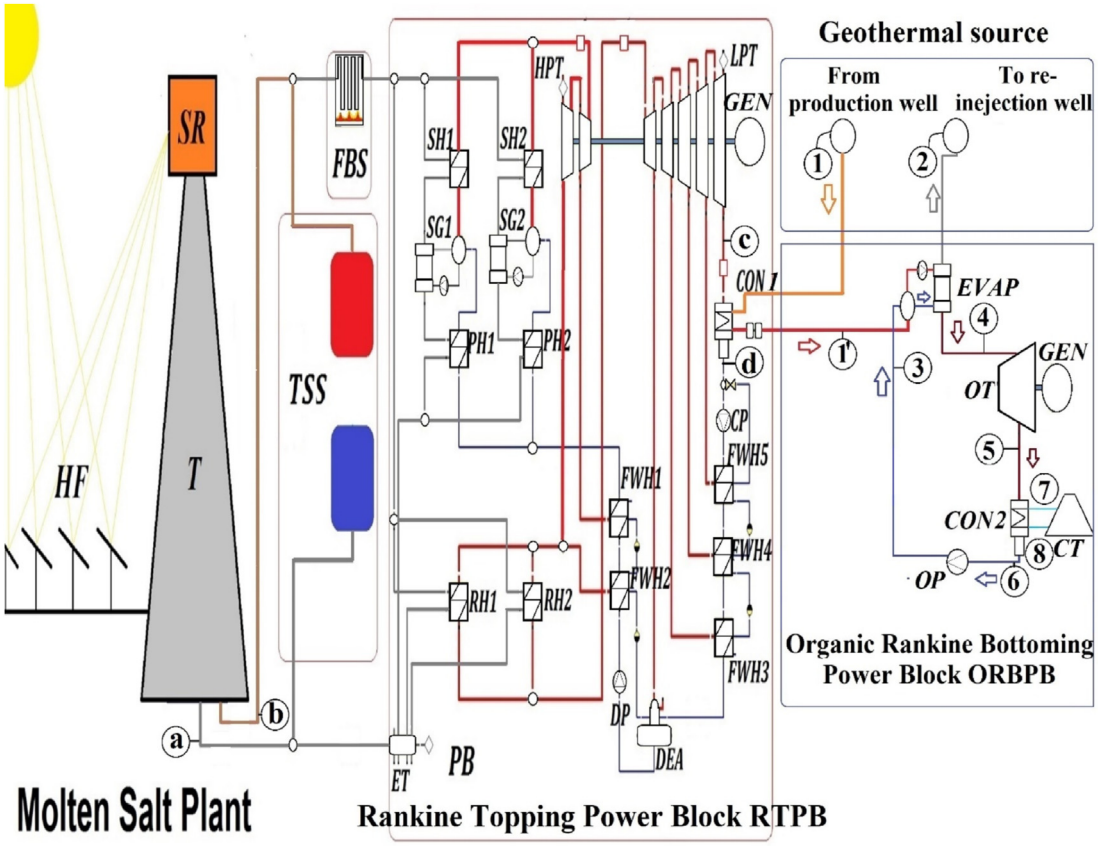

CON: Condenser, CP: Condenser Pump, CT: Cooling Tower, DEA: Deaerator, DP: Deaerator Pump, ET: Expansion tank, EVAP: Evaporator, FWH: Feed Water Heater, GEN: Generator, HPT: High-Pressure Turbine, LPT: Low-Pressure Turbine, OT: Organic Turbine, OP: Organic Pump, PH: Pre-Heater, RH: Re-Heater, SG: Steam Generator, TSS: Thermal Storage System, FBS: Fuel Backup System, HF: Heliostat Field, T: Tower, SR: Solar Receiver.

Fig. 2. Studied configuration with a topping STTPP and a bottoming BGPP.

performance of the heliostat field. The combination of these losses is presented as following [36]:

$$\eta_{opt} = \eta_{cos} \times \eta_{shad} \times \eta_{bloc} \times \eta_{ref} \times \eta_{deb} \times \eta_{dis} \quad (5)$$

where: η_{cos} marks the optical losses due to the cosine effect, η_{shad} marks the losses due to the shading effect, while η_{bloc} marks the optical losses due to the blocking effect, η_{ref} marks the losses due to reflection, while η_{deb} marks the losses due to overflow, and η_{dis} marks the losses due to dispersion.

Since a surrounding layout of the solar field is chosen in this work, it makes sense to use an external tubular receiver [37]. To better understand the thermal behavior of the solar receiver under different conditions such as received solar radiation, ambient temperature, and wind speed and direction, etc., a mathematical model is developed within System Advisor Model (SAM) software package. This model takes into consideration losses due to convection, radiation, and reflectance, in addition to the allowable flux limits. The terms included in the model can be expressed as integrals concerning axial position (x), over the length of the element (Δx), and they can be summarized as [35]:

$$\dot{q}_{HTF} = \dot{q}_{inc} - \left(\dot{q}_{ref} + \dot{q}_{rad} + \dot{q}_{conv}\right) \quad (6)$$

where $\dot{q}_{HTF}$ can be also calculated by:

$$\dot{q}_{HTF,x} = \dot{m}_{HFT} \times C_{HTF} \times \left(T_{HTF,\, x_0+\Delta x} - T_{HTF,\, x_0}\right) = U \times S_i \times \left(T_{s,x} - T_{HTF,ave,x}\right) \quad (7)$$

The heat transfer coefficient $U \times S_i$ incorporates both conduction R_{cond} (through the tube wall), and convection R_{conv} (from the inner tube wall to the HTF), and can be expressed as follows:

$$U \times S_i = \frac{1}{R_{cond} + R_{conv}} \quad (8)$$

With:

$$R_{cond} = \frac{\ln \frac{D_{o,tube}/2}{D_{i,tube}/2}}{2 \times \pi \times \Delta x \times k_{tube} \times N_{tube}} \quad (9)$$

$$R_{conv} = \frac{2}{\pi \times h_{inner} \times \Delta x \times D_{i,tube} \times N_{tube}} \quad (10)$$

The h_{inner} convective heat transfer coefficient is calculated using an empirical relation expressing the turbulent flow inside the tube [35].

The convective heat loss from the receiver to ambient is determined by:

Table 2
The main inputs of the topping STTPP [24–27].

System	Subsystem	Parameter	Value
Solar field (SF)	General working conditions	Working fluid [−]	60% $NaNO_3$+ 40% KNO_3
		Inlet working temperature [°C]	290
		Outlet working temperature [°C]	565
	Heliostat field	Heliostat surface area [m^2]	305,401
		Number of heliostats [−]	2650
		Heliostat stow deploy angle [deg]	8
	Tower and receiver	Tower height [m]	140
		Type of the receiver [−]	External receiver
		Receiver height [m]	14.22
		Receiver diameter [m]	8.89
		Number of panels [−]	16
		Tube outer diameter [mm]	40
		Tube wall thickness [mm]	1.25
		Coating emittance/absorptance [−]	0.88/0.94
Rankine topping power block (RTPB)	General working conditions	Working fluid [−]	Steam/Water
		Design turbine gross output [MWe]	19.9
		Min required temperature for startup [°C]	500
		Turbine inlet pressure control [−]	Fixed pressure
	Steam Turbine	HPT isentropic efficiency [%]	85
		LPT isentropic efficiency [%]	88
		Leaving pressure [kPa]	50
	Pumps	Feedwater P isentropic efficiency [%]	80
		Condensate P isentropic efficiency [%]	80
	Generator	Generator efficiency [%]	97
Fuel backup system (FBS)		Fossil fuel fill fraction [−]	0.27
		FBS boiler efficiency [%]	90
Thermal storage system (TSS)		Storage type [−]	Two tank molten salt
		Full load hours [hours]	15
		Tank diameter [m]	14.87
		Tank height [m]	20 m

Table 3
The main inputs of the bottoming GBPP [28–32].

System	Parameter	Value
Organic Rankine bottoming power block (ORBPB)	Working fluid [−]	R134a
	Mass flow rate of the organic fluid [kg/s]	200[a]
	Evaporative temperature [°C]	77.6
	Inlet temperature at the turbine [°C]	97.5
	Condensation temperature [°C]	18
	High pressure of the cycle [kPa]	2503
	Turbine isentropic efficiency (%)	85
	Pump isentropic efficiency (%)	80
	Generator efficiency (%)	97

[a] Assumed and it will be optimized in section 3.3.

$$\dot{q}_{conv,x} = h_m \times D_{o,tube} \times N_{tube} \times \Delta x \times \left(T_{s,x} - T_{amb}\right) \quad (11)$$

The convective heat transfer coefficient h_m is determined as the sum of forced and natural convection, and given by:

$$h_m = h_{nat} + h_{forc} \quad (12)$$

The correlations to calculate both natural (h_{nat}), and forced (h_{for}) convective heat transfer coefficients can be found in the literature [38].

The incident radiation flux on each panel with one azimuthal data point and multiple vertical data points is given by:

$$\dot{q}_{inc,x} = P_{field} \times \Delta x \times D_{o,tube} \times N_{tube} \quad (13)$$

where P_{field} is determined using the flux distribution.

While for the solar radiation reflected from the tower, and since the receiver model assumes a constant, spectrally independent, hemispherical absorptivity (α) for the tower surface, which is considered as an opaque surface, the reflectivity is 1-α, and is given by:

$$\dot{q}_{ref,x} = (1-\alpha) \times D_{o,tube} \times N_{tube} \times P_{field} \times \Delta x \quad (14)$$

For emitted solar energy from the receiver, it can be calculated as follows:

$$\dot{q}_{rad,x} = \sigma \times \varepsilon \times \pi \times \frac{D_{o,tube}}{2} \times F_{tube,s} \times N_{tube} \times \Delta x \times \left(T_{s,x}^4 - T_{amb}^4\right) \quad (15)$$

$F_{tube,s}$ is the view factor from the tube to the surroundings and takes the value 0.6366, while the emissivity ε, is taken as 0.88 [35], and σ is the Stefan-Boltzmann constant.

Regarding the exergy model, which represents the quality of energy through every stage of the energy conversion process, it can be summarized as:

The exergy received by the solar field is given by Ref. [39]:

$$\dot{E}x_{inc} = \dot{Q}_{inc} \times \left[1 - \frac{4T_{amb}}{3T_{sun}}(1 - 0.28lnf)\right] \quad (16)$$

where f is the dilution factor ($1.3*10^{-5}$) and denoted as a measure of the mixing ratio of solar radiation from the sun (T_{sun}) and radiation from the surroundings [40]. The exergy absorbed by the solar receiver ($\dot{E}x_r$) is calculated by Ref. [40]:

$$\dot{E}x_{abs} = \dot{Q}_{abs} \times \left[1 - \frac{T_{amb}}{T_r}\right] \quad (17)$$

where T_r is denoted for the temperature absorbed by the receiver.

Then, the useful exergy brought by the solar receiver is given as [40]:

$$\dot{E}x_u = \dot{m}_{SF}\left(\dot{E}x_{SF0} - \dot{E}x_{SFi}\right) = \dot{m}_f [\times (h_{HTF,0} - h_{HTF,i}) - T_{amb}(s_{SF0} - s_{SFi})] \quad (18)$$

✓ Incorporated auxiliaries (TSS and FBS)

As mentioned before, to achieve the required power generation output during low or non-solar times, integration of two auxiliaries namely TSS and FBS are highly required. The most two important technical parameters in these two systems are defined as [41]:

$$E_{tss} = \frac{w_{des}\Delta_{tss}}{\eta_{cycles\ des}} \quad (19)$$

$$f_{backup} = \frac{\dot{Q}_{FBS}}{\dot{Q}_{tot}} \quad (20)$$

$$\dot{Q}_{FBS} = \dot{m}_{HTF}(h_{in\ turbine} - h_{SFO}) \quad (21)$$

where E_{tss} is denoted for the potential number of hours that the TSS can provide energy for the operation of the RTPB, while f_{backup} presents the fossil fill fraction of the FBS.

✓ Rankine topping Power block (RTPB)

The energy model of the RTPB is based on regression equations, where heat and mass flow rates are given in normalized terms as:

$$y = f\left(\dot{m}_{HTF\ PB},\ T_{HTF},\ T_{amb}\right) \quad (22)$$

The mathematical model of SAM is carried out based on a published model presented in Refs. [42,43], where the energy efficiency of the STTPP can be written:

$$\eta_{ene,STTPP} = \frac{PG_{solar,\ net}}{\dot{Q}_{inc}} \quad (23)$$

While the exergy efficiency of the STTPP can be estimated using the following equation:

$$\eta_{exe,STTPP} = \frac{PG_{solar,\ net}}{\dot{E}x_{inc}} \quad (24)$$

The detailed model of the topping STTPP including the solar field, the thermal energy storage, and the fuel backup systems, as well as the RTPB can be found in Refs. [35,36,41–43].

2.4.2. Bottoming BGPP

In this sub-section, the mathematical modeling of the bottoming binary geothermal power plant (BGPP) is presented. According to the best of authors' knowledge and literature, taking the p-v-T behavior of the fluids, three different working fluids namely R134a, R141b, and R600a were compared in each other to be evaluated in BGPP [44,45]. These fluids were selected depending on the thermo-physical properties which are available for handled BGPP. The thermo-physical properties of these fluids are given in Table 4 [46–48].

Although R-600a seems as the best choice with its higher specific heat and lower density, R134a was chosen as the working fluid with its lower boiling point and critical temperature, and higher critical pressure which allows making more expanded designs with higher efficiencies in accordance with the technical characteristics of the geothermal source. Furthermore, this fluid is already proved its validity in many existing geothermal power plants worldwide along with its lower ozone depletion rate and global warming potential.

The mathematical model of thermodynamic analysis of the system under the assumptions of the steady-state is based on the mass balance, energy, and exergy equations. The energy rate gained by the geothermal water from the topping STTPP is given by:

$$\dot{Q}_{gain} = \dot{Q}_{rej,STTPP} = \dot{m}_{geo}(h_{1'} - h_1) \quad (25)$$

The energy transferred through the evaporator, from the geothermal source to the ORBPB can be given by:

$$\dot{Q}_{evap} = \dot{m}_{geo}(h_{1'} - h_2) = \dot{m}_{of}(h_4 - h_3) \quad (26)$$

The power generated by the expansion in the OT is calculated as:

$$\dot{W}_{OT} = \dot{m}_{of}(h_4 - h_3) \times \eta_{isen,OT} \times \eta_{Gen} \quad (27)$$

The heat rejected from the condenser of the ORBPB to the cooling tower is presented by:

$$\dot{Q}_{evap} = \dot{m}_{of}(h_{1'} - h_2) = \dot{m}_{cw}(h_8 - h_7) \quad (28)$$

While the power consumed by the pump is estimated by:

$$\dot{W}_{OP} = \dot{m}_{of}(h_3 - h_6) \times \eta_{isen,OP} \quad (29)$$

Moreover, the net generated power by the ORBPB can be presented by:

$$PG_{geo,\ net} = \dot{W}_{OT} - \dot{W}_{OP} \quad (30)$$

On the other hand, the energy efficiency of the BGPP is:

$$\eta_{ene,BGPP} = \frac{PG_{geo,\ net}}{\dot{Q}_{geo}} = \frac{PG_{geo,\ net}}{\dot{m}_{geo}(h_1 - h_2)} \quad (31)$$

While the exergy efficiency of the BGPP can be estimated using

Table 4
Properties of fluids used in system design [46–48].

Parameter	Value		
	R134a	R141b	R600a
Boiling Point (°C)	−26.1	32.1	−11.7
Freezing point	–	–	–
Critical Temperature (°C)	101.1	204.4	109.4
Critical Pressure (MPa)	4.06	4.21	3.64
Density (kg/m^3)	1190	600	540
Specific heat (kJ/kgK)	1.50	1.54	1.91

the following equation:

$$\eta_{exe,BGPP} = \frac{PG_{geo,\,net}}{\dot{E}x_{in,geo}} = \frac{PG_{geo,\,net}}{\dot{m}_{geo}[(h_1 - h_0) - T_{amb}(s_1 - s_0)]} \quad (32)$$

In the end, the global energy and exergy efficiencies of the whole combined CSP-geothermal plant can be estimated using the two equations:

$$\eta_{ene,Plant} = \frac{PG_{plant,\,net}}{\dot{Q}_{inc} + \dot{Q}_{geo}} = \frac{PG_{solar,\,net} + PG_{geo,\,net}}{\dot{Q}_{inc} + \dot{Q}_{geo}} \quad (33)$$

$$\eta_{exe,Plant} = \frac{PG_{plant,\,net}}{\dot{E}x_{inc} + \dot{E}x_{in,geo}} \quad (34)$$

While the formula of the net capacity factor of the studied hybrid plant during the whole year of operation, is given as:

$$CF = \frac{PG_{plant,\,net}}{ND.\left(24\,\frac{hr}{day}\right).19.9\,MW} \quad (35)$$

3. Results and discussion

3.1. Comparative study

The thermophysical properties of the studied configuration at the design point including, temperature, pressure, and mass flow rate, as well as enthalpy and entropy at each stage of the whole process are presented in Table 5. Furthermore, the annual comparative analysis of the two considered plants (Gemasolar plant, and the new combined plant) in term of yield and thermodynamic efficiencies, is given in Table 6, while the annual mean hourly values of energy and exergy efficiencies, as well as generated power (MW) are presented in Figs. 3 and 4 respectively.

It is well known that one of the main imperfections of CSP plants is the huge portion of wasted heat by cooling, while the new combined configuration or plant offers a good solution for this issue. As it can be noted from Table 3 and Fig. 3, by using the bottoming BGPP to convert the wasted heat from the topping STTPP, the energy efficiency of the whole plant has been decreased to 16.86%, which represent a decrease of 3.43%, while the exergy efficiency has been augmented to 22.90% respectively, which represent an increase of 30.78% compared to the conventional Gemasolar power plant. This can be justified by the boost of the generated power in the new plant, where a portion of the wasted heat from RTPB is converted to electricity in ORBPB. However, it should be pointed out that by using the new solution, the yield of the topping CSP plant has been decreased compared to the conventional plant (Table 6). This can be explained by the increase in the condensing pressure, and the decrease in the cooling performances of the RTPB (this will be further discussed in the next subsection), this will decrease the produced energy (90.27 GWh) of this side of the plant, as well as its energy (15.00%) and exergy efficiencies (15.04%).

On the other side, as it can be concluded from Figs. 3 and 4, there are varying differences between the yields of the two configurations during different hours of the day. The difference in generated power is decreasing during the period from 7:00 to 10:00 a.m., due to the decrease in energy received by the RTPB, thus, in the wasted energy converted to electricity by the ORBPB. While this difference is increasing during other periods of the day as a result of the increase in the received energy by RTPB coming from the SF, TSS, and FBS, consequently, in supplied energy to ORBPB.

3.2. Adaptation of topping BGPP to topping STTPP

For a better match, the topping STTPP dispatch levels, the mass flow rates of the organic fluid in the bottoming BGPP should be optimized. In this section of the paper, the variations of different yield indicators including annual energy and exergy efficiencies, as well as total net energy production with the variation of organic fluid mass flow rates have been presented in Figs. 5–10 for geothermal extraction temperatures vary from 50 to 120 °C respectively. Thus, different intervals of geothermal production temperature have been considered. These intervals are limited to only low-medium temperature ranges (which equivalent to low and medium enthalpy geothermal sources), to keep the high dispatch capacity of the topping solar tower thermal power plant, as an important increase in geothermal production temperatures will increase the condensing pressure of the topping plant, which leads to a remarkable drop in the generated power of this new combined plant, hence, in the yield of the hybrid plant. As can be seen from Figs. 5–10 and Table 7, the optimal mass flow rate of the ORBPB is increasing with the increase in geothermal production temperature. Its value varies from 130 kg/s for a geothermal temperature of 50 °C–310 kg/s for a source with a temperature of 120 °C. This can be explained by the increase in the energy flows reaching the ORBPB, which leads to an increasing in the optimal mass flow rate of the organic fluid to help it to convert this gained heat energy to power (Table 7). Furthermore, a very important point is the increase in the differences between energy and exergy annual efficiencies. For instance, for the low temperature of 50 °C, this difference is limited to 18.11% for annual energy efficiency and 21.35% for exergy efficiency. While this difference is increased

Table 5
Thermophysical properties of the new plant at the design point.

No	Fluid	Fluid phase	T (°C)	P (kPa)	h (kJ/kg)	s (kJ/kg.K)	$\dot{m}$ (kg/s)
a	Molten salt	Liquid	290.0	15,000	44.60	1.080	282
b	Molten salt	Liquid	565.0	3700	466.18	1.735	282
c	Water/steam	Vapor	81.3	50	2645.2	7.593	23.6
d	Water/steam	Liquid	81.3	50	340.5	1.091	23.6
1	Geo water	Liquid	65.0	240	271.5	0.892	195
1′	Geo water	Liquid	101.5	240	425.0	1.324	195
2	Geo water	Liquid	35.0	240	146.0	0.503	195
3	R134a	Liquid	53.6	2503	225.96	0.747	200
4	R134a	Vapor	118.3	2503	497.74	1.406	200
5	R134a	Vapor	109.0	537.5	457.00	1.506	200
6	R134a	Liquid	53.7	537.5	224.69	0.749	200
7	Water	Liquid	25.0	220	104.4	0.365	600
8	Water	Liquid	28.2	220	118.0	0.410	600

Table 6
Annual comparative analysis of the two considered plants.

	Gemasolar plant	New hybrid plant	Hybrid-Gemasolar (%)
$\eta_{ene,STTPP}$ (%)	–	15.00	–
$\eta_{exe,STTPP}$ (%)	–	15.04	–
$\eta_{ene,BGPP}$ (%)	–	11.84	–
$\eta_{exe,BGPP}$ (%)	–	34.59	–
$\eta_{ene,Plant}$ (%)	17.46	16.86	−3.43
$\eta_{exe,Plant}$ (%)	17.51	22.90	30.78
Capacity factor (%)	60.27	78.84	30.81
Energy production (GWh)	105.07	137.43	30.80
✓ *With Solar* contribution *(GWh)*	–	90.27	
✓ With geothermal contribution (GWh)	–	47.16	

significantly to 10.17 and 20.52% for annual energy and exergy efficiencies, respectively. These changes are due to the drop in energy efficiencies driven by the decrease in generated power of the topping STTPP (since the increase in condensing pressure of this plant), and the increase in the exploited geothermal source.

On the other side, as it can be concluded from the same Figs. 5–10, the highest energy efficiency can be obtained at the lowest geothermal extraction temperature of more than 18% (Fig. 5), while this indicator drops to the lowest value of less than

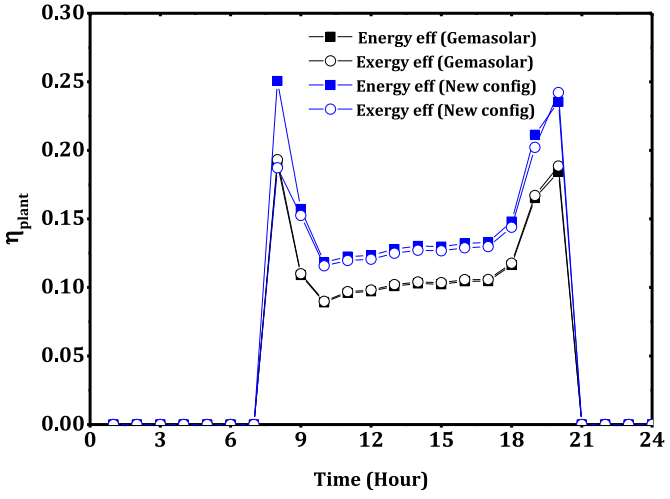

Fig. 3. Annual mean hourly energy and exergy efficiencies of the two plants.

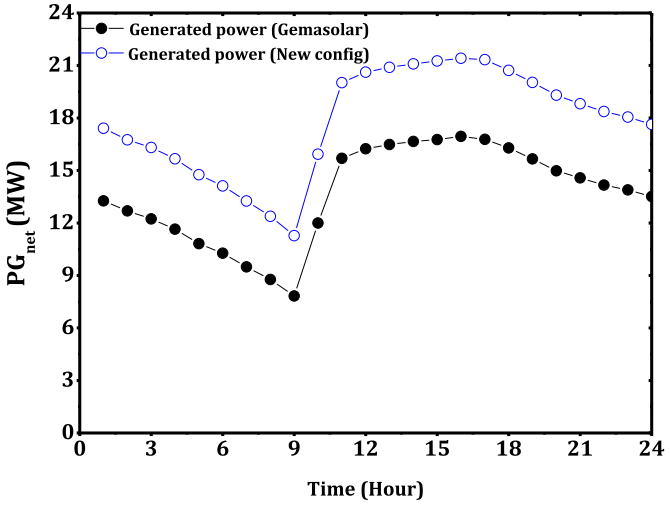

Fig. 4. Annual mean hourly generated power of the two plants.

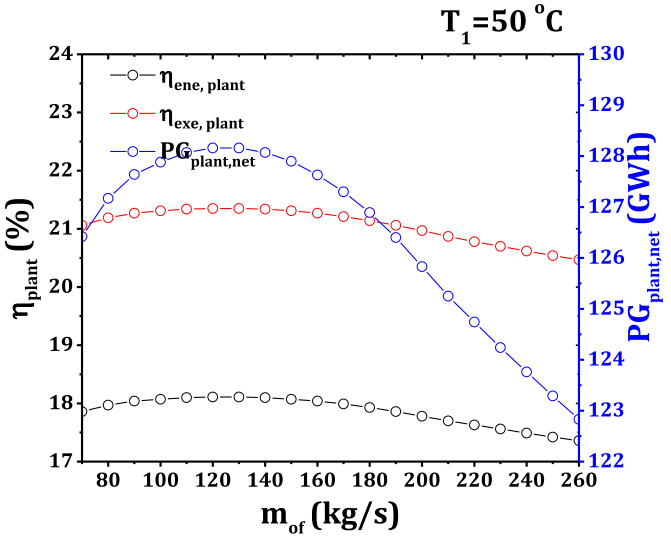

Fig. 5. Variations of η and PG_{plant} vs. variation of the mass flow rate of the organic working fluid for an extraction temperature of 50 °C.

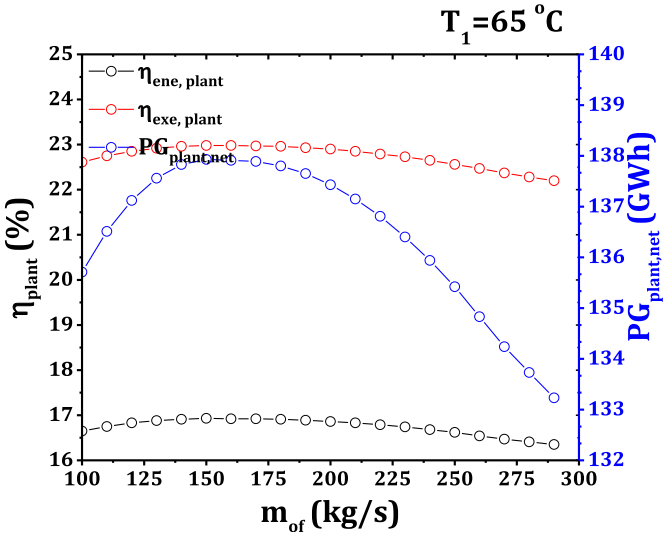

Fig. 6. Variations of η and PG_{plant} vs. variation of the mass flow rate of the organic working fluid for an extraction temperature of 65 °C.

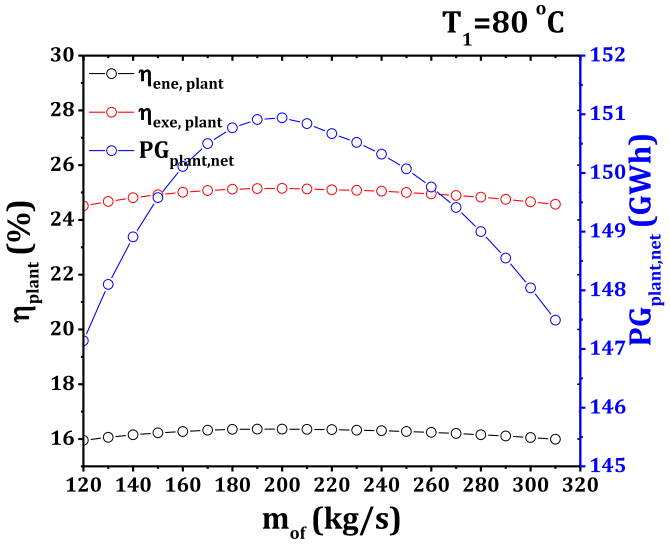

Fig. 7. Variations of η and PG_{plant} vs. variation of the mass flow rate of the organic working fluid for an extraction temperature of 80 °C.

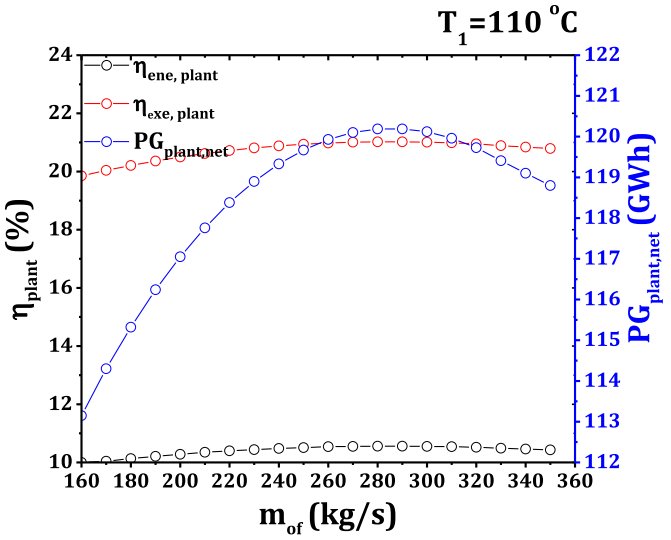

Fig. 9. Variations of η and PG_{plant} vs. variation of the mass flow rate of the organic working fluid for an extraction temperature of 110 °C.

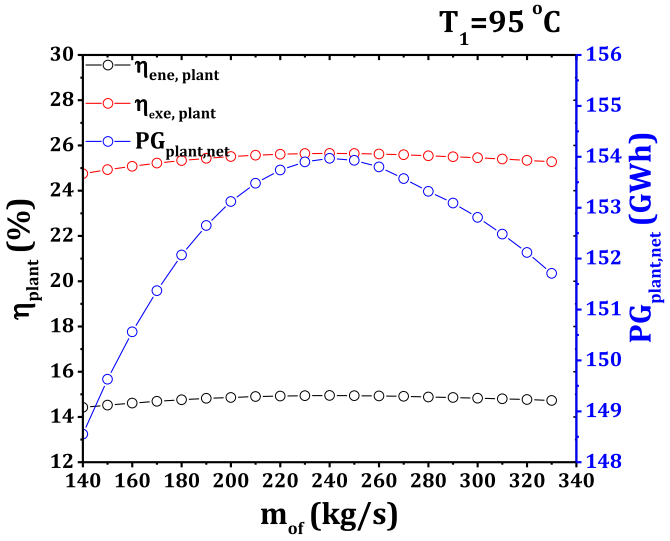

Fig. 8. Variations of η and PG_{plant} vs. variation of the mass flow rate of the organic working fluid for an extraction temperature of 95 °C.

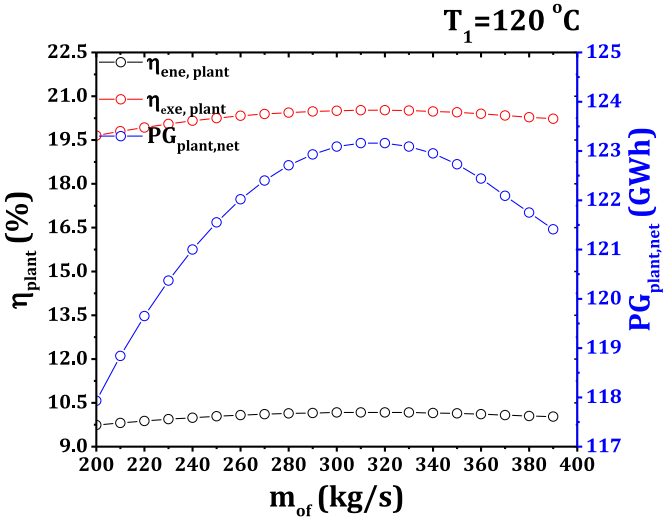

Fig. 10. Variations of η and PG_{plant} vs. variation of the mass flow rate of the organic working fluid for an extraction temperature of 120 °C.

10% for the highest geothermal temperature (Fig. 10). This can be traced back to the augmentation in the energy geothermal source that cannot be exploited by the bottoming BGPP. On the contrary, the highest exergy efficiency (more than 26%) is achieved by a relatively high extraction temperature of 95 °C (Fig. 8). The same note for the generated energy and capacity factor of the studied configuration (almost 154 GWh and 88.32% respectively). This is due to the high drop in power generation of the topping STTPP driven by the augmentation in its condensation pressure to ensure the cooling process, which is explained in the following subsection.

At the end, and as summarized in Table 7, the contribution of the topping solar plant is decreasing with the increase of the geothermal source, and in contrast to that of the bottoming geothermal plant. As it can be noted, there is a remarkable drop in generated power by the STTPP from 94.28 to 26.19 GW. This can be explained by the increase of the condensing pressure of the RTPB to ensure it's cooling by the geothermal water, while the contribution of the bottoming BGPP is increasing as the extraction temperature rises. With such configuration and such solar resources, the optimal working temperature at the geothermal source will be 95 °C, where the total generated energy and capacity factor reach 153.97 GWh and 88.32% respectively.

Table 7
Solar and geothermal contributions in the hybrid plant with the variation in the extraction temperature of the geothermal source.

Contribution	T_1 (°C)					
	50	65	80	95	110	120
$\dot{m}_{of}$ (kg/s)	130	150	200	240	280	310
$PG_{solar,net}$ (GWh)	94.28	90.27	86.15	79.35	32.15	26.19
$PG_{geo,net}$ (GWh)	33.88	47.66	64.79	74.62	88.01	96.97
$PG_{plant,net}$ (GWh)	128.16	137.93	150.94	153.97	120.19	123.16
CF (%)	73.52	79.12	86.58	88.32	68.94	70.65

4. Conclusion

In the present study, the performances of a new combined CSP-geothermal thermal power plant for large-scale power generation have been investigated. The topping CSP layout is based on the conventional solar tower power plant as that of Gemasolar with incorporated thermal storage and fuel backup systems, while the bottoming binary geothermal power plant is based on a simple layout similar to AFJET geothermal power plant, with R134a as the organic fluid. In this regard, both hourly and annual thermodynamic indicators have been considered. Furthermore, the mass flow rate of the bottoming binary geothermal with the low-enthalpy source has been optimized, to match the topping solar thermal power plant dispatch levels.

It is quite clear that this new hybrid power plant can be a good option regarding the yield dimensions, as it raises the dispatch capacity and thermodynamic performances by more than 30% compared to the conventional solar thermal power plant. Furthermore, the increase in geothermal production temperature will increase the dispatch capacity of this new hybrid plant up to almost 152 GWh annually, for a temperature of 95 °C. However, at a higher temperature, the condensing pressure of the topping solar plant will increase, which leads to a remarkable drop in the generated power of this layout, hence, in the yield of the hybrid plant.

At last, as this study presents a pre-analysis of the new plant, some weaknesses should be improved in future works including the off-design simulations of the binary geothermal power plant to avoid miscalculations of power plant performances and maintain a high level of accuracy in calculations. The choice of the best working fluids in the solar and geothermal sides should also be investigated. Furthermore, the economic dimensions should be considered to determine the feasibility of this layout in comparison to the conventional one. On the other hand, as location choice is a critical criterion to design, simulate and optimize these plants, site selection assessment is highly recommended as part of future works. In this regard, Analytical Hierarchical Process (AHP), or Geographic Information Systems (GIS) integrations can be explored.

Credit author statment

T.E. Boukelia: Writing – original draft, Methodology, Data curation, Investigation, Formal analysis; O. Arslan: Supervising, Writing – review & editing; A. Bouraoui: Visualization

Declaration of competing interest

The authors declare the following financial interests/personal relationships which may be considered as potential competing interests.

Acknowledgement

This study was supported by The Scientific and Technological Research Council of Turkey (TUBITAK) under the grant of 2221-Fellowships for Visiting Scientists and Scientists on Sabbatical Leave with the application number of 1059B211800625.

References

[1] Boukelia TE, Arslan O, Mecibah MS. Potential assessment of a parabolic trough solar thermal power plant considering hourly analysis: ANN-based approach. Renew Energy 2017;105:324–33.
[2] Astolfi M, Xodo L, Romano MC, Macchi E. Technical and economical analysis of a solar–geothermal hybrid plant based on an Organic Rankine Cycle. Geothermics 2011;40(1):58–68.
[3] Li K, Liu C, Jiang S, Chen Y. Review on hybrid geothermal and solar power systems. J Clean Prod 2019;27:119481.
[4] Zhou C, Doroodchi E, Moghtaderi B. An in-depth assessment of hybrid solar–geothermal power generation. Energy Convers Manag 2013;74:88–101.
[5] Zhou C. Hybridisation of solar and geothermal energy in both subcritical and supercritical Organic Rankine Cycles. Energy Convers Manag 2014;81:72–82.
[6] Ghasemi H, Sheu E, Tizzanini A, Paci M, Mitsos A. Hybrid solar–geothermal power generation: optimal retrofitting. Appl Energy 2014;131:158–70.
[7] Ayub M, Mitsos A, Ghasemi H. Thermo-economic analysis of a hybrid solar-binary geothermal power plant. Energy 2015;87:326–35.
[8] Cardemil JM, Cortés F, Díaz A, Escobar R. Thermodynamic evaluation of solar-geothermal hybrid power plants in northern Chile. Energy Convers Manag 2016;123:348–61.
[9] Heberle F, Hofer M, Ürlings N, Schröder H, Anderlohr T, Brüggemann D. Techno-economic analysis of a solar thermal retrofit for an air-cooled geothermal Organic Rankine Cycle power plant. Renew Energy 2017;113:494–502.
[10] Acar MS, Arslan O. Energy and exergy analysis of solar energy-integrated, geothermal energy-powered Organic Rankine Cycle. J Therm Anal Calorim 2019;137(2):659–66.
[11] Bassetti MC, Consoli D, Manente G, Lazzaretto A. Design and off-design models of a hybrid geothermal-solar power plant enhanced by a thermal storage. Renew Energy 2018;128:460–72.
[12] Bonyadi N, Johnson E, Baker D. Technoeconomic and exergy analysis of a solar geothermal hybrid electric power plant using a novel combined cycle. Energy Convers Manag 2018;156:542–54.
[13] Jiang PX, Zhang FZ, Xu RN. Thermodynamic analysis of a solar–enhanced geothermal hybrid power plant using CO2 as working fluid. Appl Therm Eng 2017;116:463–72.
[14] Keshvarparast A, Ajarostaghi SS, Delavar MA. Thermodynamic analysis the performance of hybrid solar-geothermal power plant equipped with air-cooled condenser. Appl Therm Eng 2020;5:115160.
[15] Lentz Á, Almanza R. Parabolic troughs to increase the geothermal wells flow enthalpy. Sol Energy 2006;80(10):1290–5.
[16] Lentz A, Almanza R. Solar–geothermal hybrid system. Appl Therm Eng 2006;26(14–15):1537–44.
[17] Li T, Hu X, Wang J, Kong X, Liu J, Zhu J. Performance improvement of two-stage serial organic Rankine cycle (TSORC) driven by dual-level heat sources of geothermal energy coupled with solar energy. Geothermics 2018;76:261–70.
[18] McTigue JD, Castro J, Mungas G, Kramer N, King J, Turchi C, Zhu G. Hybridizing a geothermal power plant with concentrating solar power and thermal storage to increase power generation and dispatchability. Appl Energy 2018;228:1837–52.
[19] Calise F, d'Accadia MD, Macaluso A, Piacentino A, Vanoli L. Exergetic and exergoeconomic analysis of a novel hybrid solar–geothermal polygeneration system producing energy and water. Energy Convers Manag 2016;115:200–20.
[20] Boukelia TE, Bouraoui A, Laouafi A, Djimli S, Kabar Y. 3E (Energy-Exergy-Economic) comparative study of integrating wet and dry cooling systems in solar tower power plants. Energy 2020:117567.
[21] Altun AF, Kilic M. Thermodynamic performance evaluation of a geothermal ORC power plant. Renew Energy 2020;148:261–74.
[22] https://upload.wikimedia.org/wikipedia/commons/5/59/Wilaya_d%27El_Oued.png (Last access: August, 2020).
[23] Ouali S, Hadjiat MM, Ait-Ouali A, Salhi K, Malek A. Cartographie et caractérisation des ressources géothermiques de l'Algérie. Revue des Energies Renouvelables 2018;21(1):54–61.
[24] Thirumalai NC, Ramaswamy MA. Global review of solar tower technology. Global review of solar tower. Technology. www.seriius.org/pdfs/global-review-solar-tower-technology.pdf. Last accessed: 20/5/2020.
[25] Amadei CA, Allesina G, Tartarini P, Yuting W. Simulation of GEMASOLAR-based solar tower plants for the Chinese energy market: influence of plant downsizing and location change. Renew Energy 2013;55:366–73.
[26] NREL. System advisor model (SAM) case study: gemasolar. 2013. https://sam.nrel.gov/sites/default/files/content/case_studies/sam_case_csp_salt_tower_gemasolar_2013-1-15.pdf. Last accessed: 20/10/2018.
[27] Boukelia TE, Mecibah MS, Kumar BN, Reddy KS. Investigation of solar parabolic trough power plants with and without integrated TES (thermal energy storage) and FBS (fuel backup system) using thermic oil and solar salt. Energy 2015;88:292–303.
[28] Zare V. A comparative exergoeconomic analysis of different ORC configurations for binary geothermal power plants. Energy Convers Manag 2015;105:127–38.
[29] Akman M, Ergin S. An investigation of marine waste heat recovery system based on organic Rankine cycle under various engine operating conditions. Proc IME M J Eng Marit Environ 2019;233(2):586–601.
[30] Gholizadeh T, Vajdi M, Rostamzadeh H. A new trigeneration system for power, cooling, and freshwater production driven by a flash-binary geothermal heat source. Renew Energy 2020;148:31–43.
[31] Altun AF, Kilic M. Thermodynamic performance evaluation of a geothermal ORC power plant. Renew Energy 2020;148:261–74.
[32] Bellos E, Tzivanidis C. Investigation of a hybrid ORC driven by waste heat and

solar energy. Energy Convers Manag 2018;156:427–39.
[33] Zavoico AB. Solar power tower design basis document, SAND2001-2100. Sandia National Laboratories; 2001. https://prod.sandia.gov/techlib-noauth/access-control.cgi/2001/012100.pdf. [Accessed 20 May 2020].
[34] Wagner W, Pruß A. The IAPWS formulation 1995 for the thermodynamic properties of ordinary water substance for general and scientific use. J Phys Chem Ref Data 2002;31(2):387–535.
[35] Wagner MJ. Simulation and predictive performance modeling of utility scale central receiver system power plants. Master thesis. University of Wisconsin –Madison; 2008.
[36] Rouibah A, Benazzouz D, Kouider R, Al-Kassir A, García-Sanz-Calcedo J, Maghzili K. Solar tower power plants of molten salt external receivers in Algeria: analysis of direct normal irradiation on performance. Appl Sci 2018;8(8):1221.
[37] Ho CK, Iverson BD. Review of high-temperature central receiver designs for concentrating solar power. Renew Sustain Energy Rev 2014;29:835–46.
[38] Teichel SH. Modeling and calculation of heat transfer relationships for concentrated solar power receivers. Master thesis. University of Wisconsin–Madison; 2011.
[39] Kumar KR, Reddy KS. 4-E (energy–exergy–environmental–economic) analyses of line-focusing stand-alone concentrating solar power plants. Int J Low Carbon Technol 2012;7(2):82–96.
[40] Singh N, Kaushik SC, Misra RD. Exergetic analysis of a solar thermal power system. Renew Energy 2000;19(1):135–43.
[41] Wagner MJ, Gilman P. Technical manual for the SAM physical trough model (No. NREL/TP-5500-51825). USA: National Renewable Energy Laboratory (NREL); 2001. https://www.nrel.gov/docs/fy11osti/51825.pdf. [Accessed 20 October 2018].
[42] Wagner M. Methodology for constructing reduced-order power block performance models for CSP applications: preprint (No. NREL/CP-5500-49370). USA: National Renewable Energy Lab. (NREL); 2010. https://www.nrel.gov/docs/fy11osti/49370.pdf. [Accessed 20 October 2018].
[43] Neises T, Wagner MJ. Simulation of direct steam power tower concentrated solar plant. In: 10th international conference on fuel cell science, engineering and technology. ASME; 2012. p. 499–507.
[44] Arslan O, Ozgur MA, Kose R. Electricity generation ability of the simav geothermal field: a techno-economic approach. Energy Sources Part A 2012;2012(34):1130–44.
[45] Arslan O, Kose R. Exergoeconomic optimization of integrated geothermal system in Simav. Kutahya. Energy Conversion and Management 2010;51(4):663–76.
[46] DuPont. Thermodynamic properties of R-134a. Available from: http://refrigerants.dupont.com/Suva/en_US/pdf/h47752.pdf. [Accessed 2 February 2008].
[47] Shell Chemicals. Properties of isopentane. Available from: http://www.shellchemicals.com/chemicals/pdf/solvents/hydrocarbon/paraffins/isopentane_eu_16.pdf?section=our_products. [Accessed 15 April 2007].
[48] REFPROP. Reference fluid thermodynamics and transport properties. NIST reference database. USA: National Institute of Standards and Technology, NIST; 2010., Version 9.0.